J. M. Miller, and Y. Shimamoto, Phys. Rev. 166, 949 (1968).
[5]K. Chen, G. Friedlander, and J. M. Miller, Phys. Rev. 176, 1208 (1968).
[6]*Thermal Neutron Scattering*, edited by P. A. Egelstaff (Academic, New York, 1965).
[7]E. J. Moniz, G. D. Nixon, and J. D. Walecka, in *High Energy Physics and Nuclear Structure*, edited by S. Devons (Plenum, New York, 1970).
[8]R. Hofstadter, Ann. Rev. Nucl. Sci. 7, 295 (1957).
[9]Y. Le Beyec and M. Lefort, Nucl. Phys. A99, 131 (1967); R. Bimbot and M. Lefort, J. Physique 27, 385 (1966).
[10]The calculation was actually for ^{209}Bi$(p,pn)^{208}$Bi, which is expected to be indistinguishable from that for ^{197}Au$(p,pn)^{196}$Au.
[11]H. P. Yule and A. Turkevich, Phys. Rev. 118, 1591 (1960).
[12]A. A. Caretto, U. S. Atomic Energy Commission Report No. NYO-10693, 1964 (unpublished).
[13]J. B. Cumming, Ph.D. thesis, Columbia University, New York, 1954 (unpublished); and private communication.
[14]I. Dostrovsky, Z. Fraenkel, and G. Friedlander, Phys. Rev. 116, 683 (1959).
[15]P. G. Roos, Ph.D. thesis, University of Maryland, College Park, 1964 (unpublished); and private communication from S. Wall.

PHYSICAL REVIEW C VOLUME 4, NUMBER 6 DECEMBER 1971

Resolution of Fixed-Geometry Optical-Model Ambiguities*

B. D. Watson,† D. Robson,‡ D. D. Tolbert,§ and R. H. Davis
Department of Physics, The Florida State University, Tallahassee, Florida 32306
(Received 27 August 1971)

In order to test a procedure for resolving the problem of discrete real-well-depth ambiguities found in optical-model analyses, α particles were elastically scattered from ^{70}Ge, ^{90}Zr, ^{107}Ag, and ^{140}Ce at incident energies from 0.6 to 1.2 times the classical Coulomb-barrier height for each nucleus. The real and imaginary nuclear potential-well radii and the Coulomb radius (assuming a uniformly charged sphere) for each nucleus were taken to be $R=R_C=r_0(A_{\text{Alpha}}^{1/3}+A_{\text{Target}}^{1/3})$, where $r_0=1.22$ F. A diffuseness of 0.57 F was used throughout. For three of the nuclei, only one pair of real (U) and volume-imaginary (W) potentials was found, with the real-well depth for ^{90}Zr showing a slight energy dependence. The potentials obtained were (in MeV): $U=23.5$, $W=11.0$ for ^{70}Ge; $U\sim22$, $W\sim10.3$ for ^{90}Zr; $U=25.5$, $W=14.5$ for ^{107}Ag; and $U=18.0$, $W=6.0$ for ^{140}Ce. Analysis of angular distributions taken with 15–18-MeV α particles did not yield evidence of expected ambiguities in the real-well depth, so further calculations were performed in which the effect of absorption was more generally explored. The usefulness of the proposed method was found to be limited to cases where the absorption is either ineffective, or small compared with the average spacing between single-particle levels of the same spin and parity.

I. INTRODUCTION

It is well known that optical-model analyses of elastic scattering data using the Woods-Saxon potential form factor have been unable to experimentally distinguish between several values for the real potential well depth, because nearly equivalent cross sections were predicted for each. Two types of ambiguity have been observed. Examples of the first type[1-3] were derived from analyses in which only the optical-potential strengths were variable while the Woods-Saxon geometrical form factors were held constant. A series of solutions is found for the real-potential strength, extending from about 20 to about 200 MeV and spaced by roughly 30 MeV. Potentials which are ambiguous in this discrete manner are hereinafter called type-one potentials. Previously, type-one ambiguities have been found with some certainty in the analyses of α-particle scattering from ^{24}Mg, ^{32}S, and ^{40}Ca.

Ambiguities of the second type differ from those of the first in that all parameters are free and several different real-well depths may be obtained, but only if compensating changes are made in the geometrical parameters so that the Woods-Saxon potential tails of the different optical-parameter sets effectively appear to be of nearly equivalent strength, and indeed may all converge at the "strong-absorption" radius R_{SA}.[4] The strong-absorption radius is analogous to the classical turning point for a particle with angular momentum l. In quantal terms, this radius is defined by $kR_{SA}=\eta+[\eta^2+l(l+1)]^{1/2}$. Here η is Coulomb parameter and l is the angular momentum for which $\mathrm{Re}(S_l)=\frac{1}{2}$, where S_l is the S matrix element for partial wave l. Type-two ambiguities have also been

called "continuous" ambiguities, since the optical parameters of each type-two set can usually be found to satisfy various relationships among themselves. These relationships usually vary, depending on the analysis of the particular experiment reported. Type-two potentials show little or no regularity *vis-á-vis* each other and, therefore, should not be confused with the truly discrete ambiguities of type one. Type-two phenomena have been observed mainly in scattering from nuclei heavier than mass 40.

A set of ambiguous potentials of type one and type two is also known in the literature as a "phase-equivalent" set.[5] This is because for a given partial wave, the radial wave functions for each potential well have almost identical behavior in the asymptotic region, but differ in phase by integral multiples of π in the interior region, where they are easily distinguished because of their different number of nodes. Further comments on the origin of phase equivalence appear in Sec. III.

This work attempts to resolve the question of fixed-geometry (type-one) ambiguities by applying a method suggested in the work of Eck, LaSalle, and Robson.[6] The method recognizes the fact that members of a set of type-one potentials may be distinguished, in principle, by scattering at energies below the Coulomb barrier. The potential energy differences between the tails of these real potentials should become experimentally detectable at these low energies, since the cross section is a sensitive function of the real-well depth in this energy range.[6] At higher energies, these potential-energy differences become progressively less distinguishable and thus multiple solutions may arise.

The utility of this method[6] was investigated by scattering α particles in appropriate energy ranges from targets of ^{70}Ge, ^{90}Zr, ^{107}Ag, and ^{140}Ce. For each of these nuclei, the (α,n) threshold occurs well below the energy at which the elastic scattering cross section first deviates from the Rutherford cross section. Compound elastic scattering is not expected to be significant in this case; therefore, the use of a simple four-parameter optical model should yield a fairly good representation of the experimental elastic scattering cross sections. This assumption proved to be justified, since generally excellent fits were obtained to most of the experimental excitation functions and angular distributions. The fitting procedure assumed fixed Woods-Saxon geometrical parameters and executed extensive grid searches on the real- and absorptive-potential strengths. However, no real-potential ambiguities were found, even at the highest laboratory energy (18 MeV). The ratio of absorptive potential to real potential was more than 3 times that observed in the analyses[1-3] in which type-one ambuiguities were found. Possible reasons for the absence of multiple solutions are discussed and illustrated in Sec. IV.

II. EXPERIMENTAL PROCEDURE

The experiments were carried out with α-particle beams produced by the Florida State University model EN tandem Van de Graaff accelerator. Negative helium-ion beams injected by Li vapor exchange in the source[7] easily produced accelerated He^{++} currents of 400 nA on target, if desired. Scattered α-particle yields were measured by a rotatable 16-detector ring mount[8] and by a monitor counter affixed at 20°. The angular range covered by the ring was 25–175° in the lab.

Detector pulses were sorted by a Technical Measurement Corp. (TMC) 4096-channel analyzer containing four analog-to-digital converter units, with $\frac{1}{4}$ of the analyzer memory corresponding to each. During the dead-time period of each memory section, a logic or "busy" signal was produced. Each of the four sources of busy signals together with a logic pulse derived from the monitor counter were routed to a two-input anticoincidence logic gate. The accumulated counts from each gate provided a measure of the lapsed live time of the corresponding analyzer memory section. The dead-time correction for each memory section is made by multiplying its respective peak yields by the ratio of direct monitor yield to the live-time yield from the appropriate logic gate. Further details are available.[9]

At the end of a run, the TMC memory contents were recorded by an on-line EMR 6130 computer. The peaks were displayed and marked with a light pen. The 17 pulse-height spectra together with the peak yields, live time, energy, and other run parameters were recorded on magnetic tape. Data reduction and analysis were carried out with the aid of a CDC 6400 computer.

The target nuclei chosen to test the type-one selection technique are reasonably spherical (on a shell-model basis) and the reaction Q values are such that the elastic scattering cross sections were not expected to exhibit compound-nuclear effects. The targets selected were ^{70}Ge, ^{90}Zr, ^{107}Ag, and ^{140}Ce. Compound elastic processes should be insignificant for these targets because: (1) For incident energies below the Coulomb barrier, penetration is weak for many partial waves whose phase shifts contribute significantly to the elastic cross section; and (2) as the energy increases, flux entering the nuclear volume should leave through reaction channels (especially neutrons) at an increasing rate. Energy averaging of the

differential cross section was accomplished by using targets from about 0.8 to 2.4 mg/cm^2 thick, corresponding to averaging the beam over at least a 170-keV interval at all energies. The isotope material was obtained from Oak Ridge National Laboratory, Isotope Sales Division. Other target information is presented in Table I.

In order to accurately compare the data with theoretical calculations, expressions for the mean incident beam energy and the energy-averaged Rutherford cross section were derived using an empirical formula[10] for α-particle energy loss in thick targets. The relative error between different angular distributions taken at the same energy was minimized by measuring the target thickness anew for each angular distribution. This was possible because at most energies for each nucleus there was at least one angle for which Rutherford scattering could be expected.

The use of the energy-loss formula[10] is valid because of the small effect of straggling on the actual energy distribution of particles leaving each lamina of the target. This distribution was calculated to be a Gaussian; hence the average is equal to the most probable energy, in contrast to the general Landau-Symon shape for which the calculation of the average energy at each lamina is rather complicated.[11]

III. THEORY

A. Optical-Model Formalism

The local optical model assumes that a central, two-body interaction between the centers of mass of the target and projectile can represent a reasonable average interaction for the many-body elastic scattering problem.[12] The optical potential used during most of this work is of the simple form[13]

$$V^{\mathrm{OM}}(r) = -(U + iW)f(r,R,a) + V_C, \qquad (1)$$

where

$$f(r,R,a) = [1 + e^{(r-R)/a}]^{-1}$$

and

$$V_C = \begin{cases} \dfrac{Z_p Z_t e^2}{2R_C}\left[3 - \left(\dfrac{r}{R_C}\right)^2\right] & r \le R_C \\ \dfrac{Z_p Z_t e^2}{r} & r > R_C . \end{cases}$$

Here U and W are the real- and imaginary-well depth parameters, respectively, R is the half-density radius, and a is the "diffuseness" parameter. The term V_C is the electrostatic potential of a uniformly charged sphere of radius R_C, and Z_p and Z_t are the charges of the projectile and target.

The thick targets used provided the energy averaging necessary for analysis with the phenonemological optical model. The inclusion of a compound elastic term[14] and/or an angular-momentum-dependent imaginary absorption[15] in the cross section did not enhance the fit to the data significantly.

B. Discrete Optical-Model Ambiguities

The existence of discrete ambiguities in the optical potentials for strongly absorbed particles was first noted by Drisko, Satchler, and Bassel.[5] The purpose here is to discuss the origin of type-one ambiguities and how they are affected by the magnitude of the absorption W.

The conditions for ambiguity of two potentials are illustrated in Fig. 1. A spectrum of bound and unbound resonant states exists in each potential formed by superposition of the attractive real optical potential and the repulsive Coulomb and centrifugal potentials. (The contribution of the latter potential is not shown, since it is different for each partial wave). The ordering of these states is roughly analogous to the eigenstates of a harmonic-

TABLE I. Thickness and energy loss for ^{70}Ge, ^{90}Zr, ^{107}Ag, and ^{140}Ce targets.

Isotope	Purity (%)	Average thickness (mg/cm^2)	Method of preparation	Energy loss at E_{lab} = 15 MeV (MeV)	Mean energy E_m at E_{lab} = 15 MeV (MeV)
^{70}Ge	92.8	0.82	Evaporation onto C target backings	0.19	14.91
^{90}Zr	97.8	1.25	Rolled by ORNL	0.26	14.85
^{107}Ag	99.8	2.17	Evaporation, self-supporting	0.42	14.77
^{140}Ce	99.0	2.38	Evaporation, of $^{140}CeO_2$ onto C target backings	0.62	14.69

oscillator (HO) potential except that the above potential removes the l degeneracy. It should be kept in mind that the finite potential has resonant states in the continuum with eigenvalues which are indeterminate because of the natural widths Γ of the states.[5] The radial functions representing such resonant states have not been uniquely defined in the literature, but for simplicity each can be evaluated at an energy corresponding to the center of its resonant behavior. These potential resonances may be "observed" by calculating excitation functions for the case of no absorption, i.e., $W=0$.

The splitting of the "HO" eigenstates into several components satisfying the condition $2n+l-2=N$ is shown in Fig. 1, as are qualitative examples of the real or imaginary radial wave function corresponding to each level. Here N is the major oscillator quantum number, while n is the number of nodes (in nuclear notation the point at the origin is counted as a node) in a radial eigenfunction corresponding to angular momentum l. "Phase equivalence" becomes possible when the different well depths are adjusted such that families of states with the same parity (i.e., differing in N by multiples of 2) are located at the same energy relative to an incident beam, even though the aligned families of states are different in number. For example, Fig. 1 shows that there is no analog in well (a) for the $l=4$ level shown in well (b). The eigenfunctions of states having the same l values in the corresponding wells are phase-shifted by multiples of π inside the well, but are "phase equivalent" in the asymptotic region. Equality of cross sections calculated using different phase-equivalent wells would be violated in the unlikely situation where those states with high-l values of certain wells, which do not have counterparts in other wells at the same approximate energy, yield phase shifts

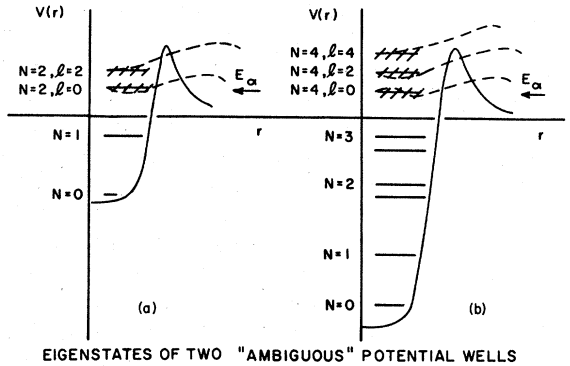

FIG. 1. Typical eigenstates of two ambiguous real potential wells. Qualitative examples of the real or imaginary radial wave function corresponding to each level are shown. The cross-hatching indicates the uncertainty in the energy of each unbound state.

which appreciably affect the scattering amplitude.

When a small absorptive potential of strength W is included, each resonant state assumes a Lorentzian energy spread of width roughly $\Gamma+2W$.[16] The smallness of W is best determined relative to the spacing (Δ) of the nearby resonant states in the potential. One can naively define the "level-level interference" as the area (energy units) of overlap between two neighboring resonances relative to the overlap of each resonance with itself, i.e.,

$$g_{n,n+1}=\frac{(W/\Delta_n)^2}{\frac{1}{4}+(W/\Delta_n)^2}\,. \tag{2}$$

In this simple estimate the levels are assumed to have equal residues or reduced widths – a valid approximation for s-wave square wells. Therefore, the extent to which the levels (defined for $W=0$) interfere with each other, or "mix," depends on the ratio W/Δ. For a square-well radius R the level spacing for s waves is estimated as

$$\Delta_n=E_{n+1}-E_n=n\left(\frac{\hbar^2\pi^2}{mR^2}\right), \tag{3}$$

and, consequently, Δ_n increases as the well depth increases owing to more nodes occurring in the resonant states. Similar behavior is expected for a Woods-Saxon potential.

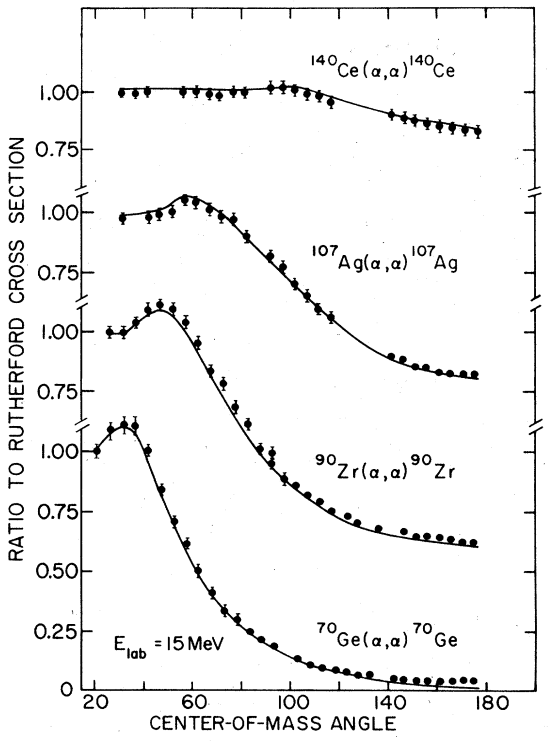

FIG. 2. Angular distributions at $E_{lab}=15$ MeV. Fitting parameters are given in Table II.

Type-one ambiguities are expected to occur when W/Δ is small, since the levels are only weakly mixed and essentially maintain their isolated level character. Since Δ increases as the well depth increases, phase equivalence occurs only by also increasing W. In this way the level mixing is kept equivalent for each of the phase equivalent real potentials. This situation was observed in all of the earlier work[1-3] on type ones.

If W becomes comparable to the average level spacing, the corresponding "major oscillator" bands of the ambiguous potential wells become overlapping and, if W is further increased, the band structure disappears completely. When this happens, levels of the same spin and parity, but originally belonging to different "oscillator" bands, will mix according to the Breit-Wigner many-level formula.[17] States mixed in this manner exert different effects on the cross section predicted by the various potential wells, since each well binds differing numbers of "oscillator" bands and, hence, contains different numbers of levels of the same spin and parity. Therefore, it should be possible to select one well depth experimentally, since they are now all distinct.

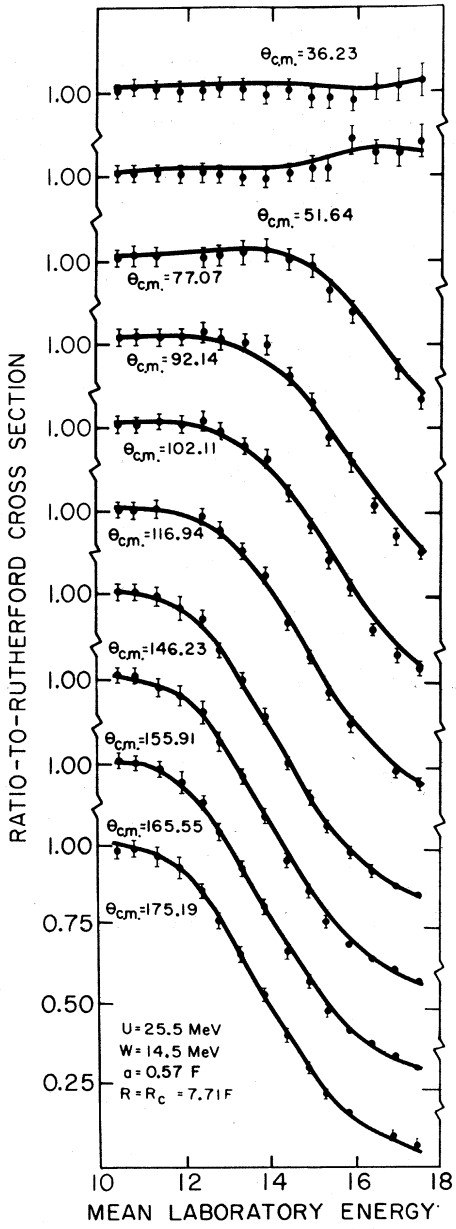

FIG. 3. $^{107}Ag(\alpha,\alpha)^{107}Ag$ excitation functions.

IV. EXPERIMENTAL RESULTS AND ANALYSIS

A. Presentation of Fitted Data

The optical parameters were varied in order to obtain those parameter sets whose corresponding cross sections gave the best agreement with the experimental results. The fitting criterion used was the minimization of χ^2, where

$$\chi^2=\frac{1}{N}\sum_{i=1}^{N}\left\{\left[\frac{d\sigma(\theta_i)}{d\Omega}\right]_e-\left[\frac{d\sigma(\theta_i)}{d\Omega}\right]_c\right\}^2\Big/\left[\Delta\frac{d\sigma(\theta_i)}{d\Omega}\right]_e^2. \tag{4}$$

The subscripts e and c label the experimental and the computed cross sections, respectively, while the error in the experimental cross section at angle θ_i is given by $\Delta[d\sigma(\theta_i)/d\Omega]_e$. Searches for minimum χ^2 were carried out on angular distributions taken at N angles. The simple four-parameter optical model was found to represent most of the data very well; hence the reasons for ignoring further parametrization of the model (see previous section) appear to be justified.

A consistent geometry was used throughout the analysis. The diffuseness was assumed to be 0.57 F for each nucleus, and the optical half-way radii were determined from $R=r_0\,(A_{\text{Alpha}}^{1/3}+A_{\text{Target}}^{1/3})$, where $r_0=1.22$ F. The nuclear-charge distribution was assumed to be that of a uniformly charged sphere of radius R_C, where for simplicity the Coulomb radii (R_C) were taken equal to the real-well half-way radii. This choice of parameters was thought to be acceptable for the purpose of discriminating between real-well depths for a fixed geometry, since they are comparable to phenomenological size parameters appearing in the literature. All theoretical cross sections were calculated at the target-averaged mean energy in the center-of-mass coordinate system, thus yielding direct comparison with the experimental center-of-mass cross sections. Averaged cross sections were

TABLE II. Results of optical-model-parameter searches on angular-distribution data.

Target	Laboratory bombarding energy (MeV)	Radius, diffuseness (F)	χ^2 at highest energy listed	Real-well depth (MeV)	Imaginary-well depth (MeV)
^{70}Ge	8.0–15.0	6.96, 0.57	12.0	23.5	11.0
^{90}Zr	8.0–18.0	7.41, 0.57	21.9	23.5	10.2
^{107}Ag	10.5–18.0	7.71, 0.57	3.2	25.5	14.5
^{140}Ce	13.0–17.5	8.26, 0.57	0.3	18.0	6.0
^{90}Zr	17.0	7.20, 0.47	19.5	216.0	19.0

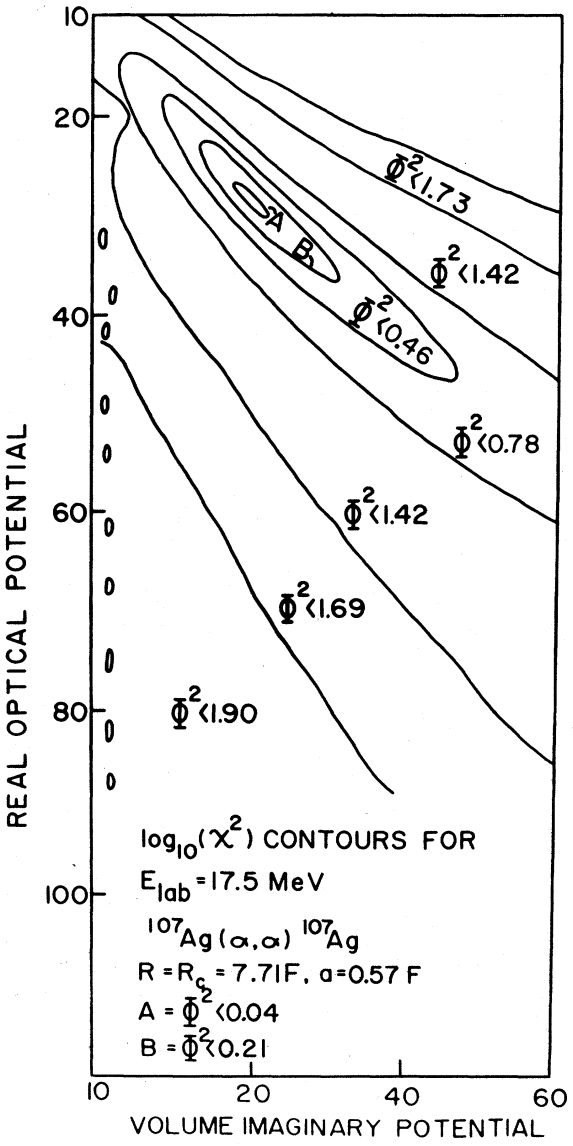

FIG. 4. χ^2 contours for ^{107}Ag$(\alpha,\alpha)^{107}$Ag at E_α(lab) = 17.5 MeV. Here χ^2 is displayed as Φ^2, where $\Phi^2 = \log_{10}(\chi^2)$. The small unlabeled contours along the ordinate represent local minima for which $\Phi^2 \sim 1.7$.

also computed by dividing the target thicknesses into lamina and then applying Simpson's rule. These results differed from the above by less than 0.5%.

In general the absolute experimental error for each nucleus was an estimated ±4%. About ±3% of this was due to the error in measuring the average target thickness for each angular distribution. A significant component of the error was due to the uncertainty in detector angle caused by horizontal fluctuations of the beam across the face of the target. This error varied from about 1% at the forward angles to about 0.5% at the backward angles.

Exemplary optical-model fits to the data are shown in Figs. 2 and 3. Only one pair of real and imaginary optical potentials is required, for three of the four nuclei listed in Table II, to fit all of the data. The ^{90}Zr higher-energy data preferred a real potential of about 23.5 MeV and the lower-energy data preferred the shallower potential of about 20 MeV. In general, the data for ^{90}Zr appear to indicate an energy-dependent U. However, this effect may be spurious as there was some difficulty in determining the normalization very accurately over the energy range displayed, owing to target impurities.

The results of extensive searches on the real and imaginary potentials, keeping the geometry fixed, for the highest-energy angular distribution for each nucleus are shown in Fig. 4 and Table II. The contours of constant χ^2 (drawn here as $\Phi^2 = \log_{10}\chi^2$) formed a similar pattern for each case. As shown in the representative contour of Fig. 4, there is only one region in which χ^2 is a minimum. This was surprising, since on the basis of previous work,[1-3] real-well ambiguities were found at these energies. The angular distribution at 17.0 MeV for ^{90}Zr was reanalyzed with a different well geometry in order to see if the parameters a and R were responsible for the character of the χ^2 surfaces. This was not the case; the results are listed in Table II. Also, it seems evident that the character of the χ^2 surfaces is not critically determined

by the precision of the data, since all these surfaces assumed a rather monotonic behavior outside the minimum region, with no evidence of any other significant depressions. The small unlabeled contours seen in Fig. 4 are discussed in Sec. IV B.

B. Search for Real-Potential Ambiguities

A search for higher-energy data was undertaken as it was thought that possibly the Coulomb barrier was still able to mask the existence of ambiguous potentials. Analyses of 24.7-MeV data[18] and 40-MeV data[19] for the scattering of α particles from ^{107}Ag yielded optical parameters from which cross sections could be reconstructed, at least to the accuracy to which the optical model represents the data. The analysis of the 24.7-MeV computed "data," keeping the same geometry as before and assuming "experimental error" of 8% at all angles, produced the same behavior as that exhibited in Fig. 4. Fits to the 40-MeV reconstituted data were not good for any values of real and imaginary potentials. Many local minima were found but none of these had χ^2 values less than 20; thus this latter analysis offered no satisfactory evidence for the "missing" potentials.

Some recent analyses[20,21] of very high-energy α scattering have also found a unique pair of real and imaginary potentials. The absorption used in each case was greater than 17 MeV. Apparently potential wells, which would be ambiguous if the absorption required by the data were a small fraction of U, become distinct when the required absorption is a large fraction of U. When the absorptive strength is at least as large as the average "major-oscillator" level spacing in each of the ambiguous potential wells, the contribution to the cross section of levels located at energies far removed from the incident beam energy can become significantly different for different well depths. Under these conditions the method suggested in Ref. 6 may not be needed.

C. Ambiguity Criteria from a Simple Model

A simple calculation was performed which adequately displays the absence of observable multiple solutions for the real potential in the presence of large absorption. Assuming s waves incident on a complex attractive square-well potential, the Schrödinger equation is solved in the usual manner to obtain continuity of the logarithmic derivative at the matching radius r:

$$R(r)=\frac{e^{ikr}-Se^{-ikr}}{e^{ikr}+Se^{-ikr}}\ \frac{1}{ikr}=\frac{\tan(A+iB)}{A+iB}\,, \tag{5}$$

where R is the complex R function of R-matrix theory, k the external wave number, and S the S-matrix scattering amplitude. The parameters A and B are given by

$$A=(\sqrt{m}\,r/\hbar)f\,, \tag{6}$$

$$B=\frac{\sqrt{m}\,r|W|}{\hbar}\,\frac{1}{f}\,, \tag{7}$$

where

$$f\equiv f(|U|+E,|W|)=\{|U|+E+[(|U|+E)^2+|W|^2]^{1/2}\}^{1/2}\,, \tag{8}$$

and $A+iB=Kr$ with K being the complex internal wave number.

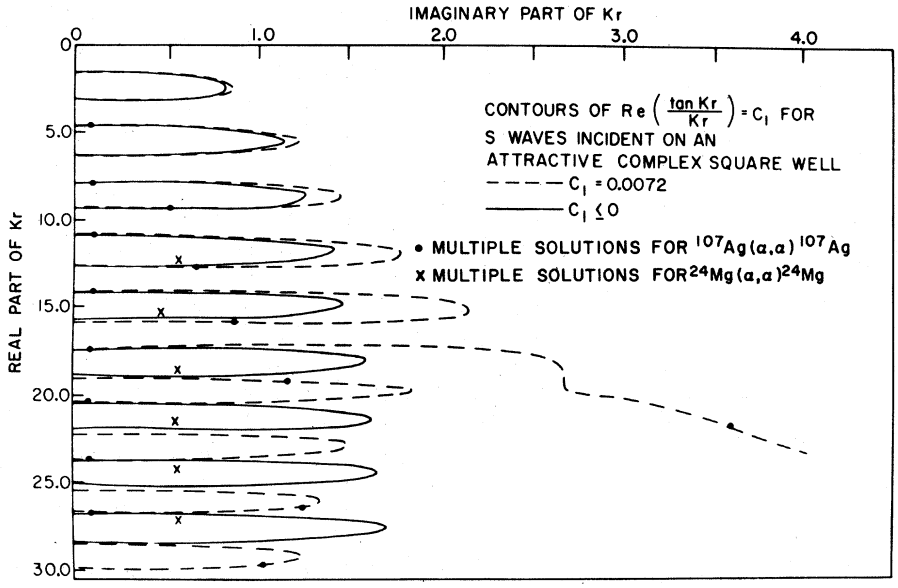

FIG. 5. Contours for the real part of the R function for an attractive complex square well.

Thus for an incident energy E, a pair (A, B) defines a unique pair $(|U|, |W|)$ from which the S matrix element can be evaluated. If a particular pair of (A, B) denoted by (A_1, B_1) is selected, the question of phase-equivalent ambiguities is now reduced to the question: For what other pairs of (A, B) is the relation $R(A, B) = R(A_1, B_1)$ possible? The real and imaginary parts of $R(A, B)$ must simultaneously equal their counterparts in $R(A_1, B_1)$.

The problem is best solved by overlaying and aligning two graphs, one representing the contours of $\mathrm{Re}[R(A, B)] = c_1$ and the other the contours of $\mathrm{Im}[R(A, B)] = c_2$, where c_1 and c_2 are constants. The pairs of (A, B) that designate the same value of $R(A_1, B_1) = c_1 + ic_2$ are given by the points at which the contours defined by c_1 and c_2 intersect. This is illustrated in Figs. 5 and 6. A starting pair of $(A, B) = (22.25, 3.7)$ was derived from analysis of the experiment $^{107}\mathrm{Ag}(\alpha, \alpha)^{107}\mathrm{Ag}$ at 17.5 MeV. Figure 5 shows the locus points satisfying $\mathrm{Re}[R(22.25, 3.7)] = 0.0072$ and regions enclosed by solid lines satisfying $\mathrm{Re}[R(A, B)] \leq 0$. The points marked by $\times$ are discussed below. Figure 6 shows the contours $\mathrm{Im}[R(22.25, 3.7)] = 0.0405$. The pairs of (A, B) giving $R(A, B) = 0.0072 + 0.0405i$ are shown as dots on the graph of $\mathrm{Re}[(A, B)]$, Fig. 5. The existence of these extra "solutions" is discussed below.

If analysis of the data indicates that a set of optical parameters can be found, and if the pair (A_1, B_1) calculated from these yields $\mathrm{Re}[R(A_1, B_1)] \leq 0$, then other equivalent sets are confined to those successive regions satisfying $\mathrm{Re}[R(A, B)] \leq 0$, $A \neq A_1$. This pattern of solutions occurs for B (and hence W) small. Indeed, the pairs of (A, B) calculated with the type-one potentials found in Refs. 1–3 were found to approximately satisfy these conditions in each case. The pairs of (A, B) derived from analysis[1] of the reaction $^{24}\mathrm{Mg}(\alpha, \alpha)^{24}\mathrm{Mg}$ are marked by $\times$ in the regions of Fig. 5 where $c_1 < 0$. That these solutions are phase-equivalent is conveniently shown because the points $\times$ are spaced by about π in the A coordinate, i.e., the equivalent real phase shifts are π apart.

Very different behavior is observed when $\mathrm{Re}[R(A, B)] > 0$, an example of which is sketched in Figs. 5 and 6. Figure 5 shows that all of the points representing $R(A, B) = 0.0072 + 0.0405i$ are phase-equivalent in the above-mentioned sense except for one anomalous point for which B (and hence W) is appreciably larger than the B values observed for the other points. It is interesting to note that increasing the incident energy E does not necessarily create conditions for phase equivalence because of the energy dependence in the absorption W. For example, $(A, B) = (22.25, 3.7)$ could also represent the situation corresponding to the reaction $^{40}\mathrm{Ca}(\alpha, \alpha)^{40}\mathrm{Ca}$ at 70 MeV using a radius of 5.2 F, a real potential of 25 MeV, and an energy-dependent W given by $W = 0.46\,(E_\alpha - 1.4)$ as found in Ref. 3. Thus, for the possibility of this "uniqueness" condition to arise, the data must require a relatively large absorptive potential defined approximately by $B \geq \pi$ for which $\mathrm{Re}[R(A, B)]$ is never ≤ 0.

Certainly not all of the solutions predicted by this model were observed in this experiment; the contours of χ^2 (see, for example, Fig. 4) indicate that just one solution was found for each nucleus. However, some various local minima were observed in the analyses of $^{107}\mathrm{Ag}$ and $^{140}\mathrm{Ce}$ data. Figure 4 shows this for $^{107}\mathrm{Ag}$ by the unlabeled contours located in the region of small W. The χ^2 values for these were much worse by at least a factor of

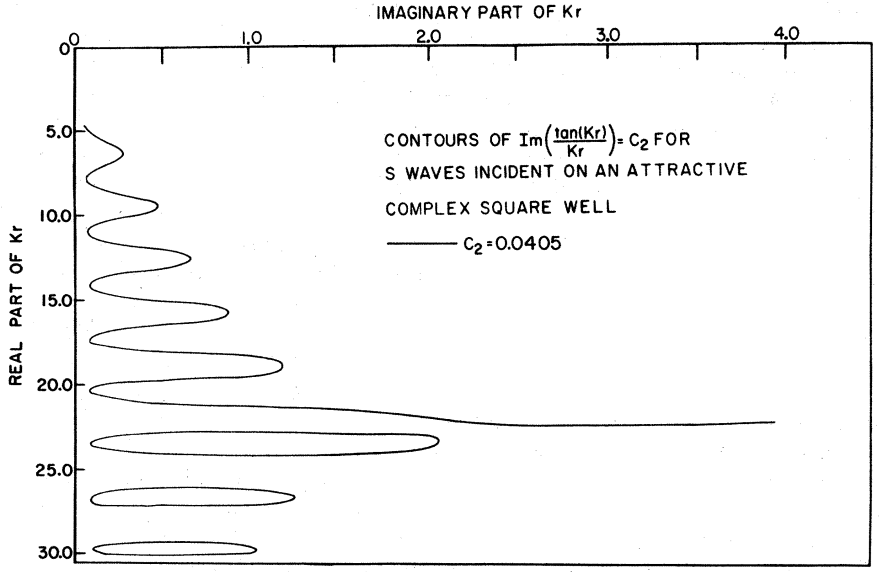

FIG. 6. Contours for the imaginary part of the R function for an attractive complex square well.

10, than those due to the "unique" solutions. It does appear, however, that the simple model used here does predict the existence of these extra "solutions," but only qualitatively. The most important feature predicted is the existence of one solution which is evidently not related in any simple way to these other "solutions." This solution is apparently very stable with respect to changes in the energy, potential depth, and absorption, since the real and imaginary parts of the R function assume a smooth monotonic behavior for $\beta > \pi$, and partial derivatives with respect to A or B are nearly zero. The derivatives of the R function of the other "solutions" are considerably greater, and for the s-wave situations studied here they are sufficiently large to term these solutions "unstable." Phase equivalence for the unstable solutions will not occur *simultaneously* for all partial waves, since a small change in A or B causes larger changes in the R function (and therefore, in the cross section). This instability is further enhanced for solutions corresponding to small B when the normal Woods-Saxon well is used. However, relatively stable solutions result if the condition $\mathrm{Re}[R(A,B)] < 0$ is satisfied by each solution, as shown by the ^{24}Mg analysis.

V. SUMMARY AND DISCUSSION

Type-one ambiguities are expected in analyses of scattering at medium energies from nuclei whose reaction threshold Q values for light-particle production are high, especially with respect to the energy at which the cross section first breaks from the Rutherford cross section. These analyses require only small absorption, since the relatively few open reaction channels in each case are able to carry off only a small fraction of the flux made available in the incident channels. Examples of such nuclei have already been mentioned, namely, $4n$ nuclei, where n is the number of α-particle clusters in the nucleus. Type-one ambiguities may be resolved by scattering at low energies, where the real Coulomb barrier selects a real-well depth, or removed at high energies, where the increased absorption distinguishes all the possible real-well depths from each other. Although the former case has not yet been studied for any of the $4n$ nuclei, the latter case was observed in the analysis[21] of ^{24}Mg$(\alpha,\alpha)^{24}$Mg at 40 and 80 MeV.

All of the above should apply to the scattering of any composite projectile (that is any projectile heavier than a nucleon), even those normally thought to be "strongly" absorbed, because the absorption depends most importantly on the number of final states made available in the *residual* nuclei. If the target nucleus is not a $4n$ nucleus, then it is probable that the absorption will be large enough to preclude observation of type-one ambiguities. A verification of this for light nuclei (e.g., ^{9}Be) would be interesting, particularly at low energies.

Evidently the roles played by the Coulomb barrier and the absorption are equivalent in some sense, since the type-one ambiguity is removed by either, depending on the incident energy. This "equivalence" was indicated by calculations of the total and partial wave functions. If either the absorption or the Coulomb barrier is effective in determining the real potential, the total and partial wave functions calculated for either case are qualitatively the same in that their magnitudes inside the well radius are very small. This is because on the one hand, the Coulomb barrier does not allow significant penetration of partial waves whose phase shifts contribute to the scattering. On the other hand, in the limit of large absorption, partial waves incident at higher energies are greatly attenuated in the interior. This indicates that only the tail region of the potential, i.e., the nuclear surface, is significant in determining a unique value for this potential.

When the absorption is large other solutions for the real-well depth can be obtained only if the well geometry is varied. These solutions correspond to the type-two ambiguities mentioned earlier. For large W, only the surface region is critical for type-two potentials which, as discussed in Sec. I, have tails of very similar strengths. This was verified by obtaining fits to the present data for ^{107}Ag$(\alpha,\alpha)^{107}$Ag using potential parameters derived from an analysis[19] at higher energies. The fits obtained were as good or better than the fits shown in Figs. 2 and 3.

The real-well depths obtained in this work were quite shallow and considerably less than the often used well depth of ~200 MeV "deduced" from nucleon scattering. As indicated in Table II, it is possible to obtain a fit to the data with a real-well depth of ~200 MeV; however, one must assume a rather unlikely diffuseness (typically $a < 0.5$). There exists a definite relationship between the free-state optical potential and the bound-state potential. This relationship was necessary for nucleons in order to eliminate type-one ambiguity and required an optical-well depth of ~50 MeV, since it was already known that such a well gives the right number of bound states for nucleons. The analogous situation for composite particles has not been explored properly so far and requires future experiments on composite-particle pickup, stripping, and knock-out reactions to provide the appropriate bound-state information.

ACKNOWLEDGMENTS

The authors wish to thank Dr. J. P. Aldridge and Dr. W. J. Thompson for valuable discussions, and Dr. A. E. Bisson, Dr. W. J. Wallace, Dr. K. A. Eberhard, J. W. Frickey, K. R. Knuth, and R. W. Hamm for their assistance in making the measurements.

---

*Research sponsored in part by the Air Force Office of Scientific Research, Office of Aerospace Research, United States Air Force, under AFOSR Grant No. AF-AFOSR-69-1674, and the National Science Foundation Grant No. GJ-367.

†Present address: Institute of Molecular Biophysics, Florida State University, Tallahasseè, Florida.

‡Alfred P. Sloan Fellow.

§Present address: University Hospital, University of Wisconsin, Madison, Wisconsin.

[1]W. J. Thompson, G. E. Crawford, and R. H. Davis, Nucl. Phys. A98, 228 (1967).

[2]J. P. Aldridge, G. E. Crawford, and R. H. Davis, Phys. Rev. 167, 1053 (1968).

[3]C. P. Robinson, J. P. Aldridge, J. John, and R. H. Davis, Phys. Rev. 171, 1241 (1968).

[4]J. S. Blair, Phys. Rev. 95, 1218 (1954); 108, 827 (1957).

[5]R. M. Drisko, G. R. Satchler, and R. H. Bassel, Phys. Letters 5, 347 (1963).

[6]J. S. Eck, R. A. LaSalle, and D. Robson, Phys. Letters 27B, 420 (1968).

[7]K. R. Chapman, Nucl. Instr. Methods 73, 255 (1969).

[8]E. Feldl, P. Weiss, and R. H. Davis, Nucl. Instr. Methods 28, 309 (1964); J. P. Aldridge, G. E. Crawford, and R. H. Davis, Phys. Rev. 167, 1053 (1968).

[9]B. D. Watson, Ph. D. dissertation, Florida State University, 1970 (unpublished).

[10]V. E. Lewis, Nucl. Instr. Methods 64, 293 (1968).

[11]B. Rossi, *High Energy Particles* (Prentice-Hall, Englewood Cliffs, New Jersey, 1956), Chap. 2, pp. 22–35.

[12]H. Feshbach, C. E. Porter, and V. F. Weisskopf, Phys. Rev. 96, 448 (1954).

[13]R. W. Woods and D. S. Saxon, Phys. Rev. 95, 577 (1954).

[14]I. Úlehla, L. Gomolčak, and Z. Pluhář, *Optical Model of the Atomic Nucleus* (Academic, New York, 1964), Chap. 3, pp. 65–75.

[15]A. E. Bisson and R. H. Davis, Phys. Rev. Letters 22, 542 (1969).

[16]A. M. Lane, R. G. Thomas, and E. P. Wigner, Phys. Rev. 98, 693 (1955).

[17]G. Breit and E. P. Wigner, Phys. Rev. 49, 519, 642 (1936).

[18]L. McFadden and G. R. Satchler, Nucl. Phys. 84, 177 (1966).

[19]M. El Nadi and A. Riad, Nucl. Phys. 65, 99 (1965).

[20]I. Brissaud, M. K. Brussel, M. Sowinski, and B. Tatischeff, Phys. Letters 30B, 324 (1969).

[21]P. P. Singh, R. E. Malmin, M. High, and D. W. Devins, Phys. Rev. Letters 23, 1124 (1969).

PHYSICAL REVIEW C VOLUME 4, NUMBER 6 DECEMBER 1971

Absolute Cross Sections for 2-keV Neutron Capture in ^{204}Pb and ^{207}Pb†

R. C. Greenwood and C. W. Reich

National Reactor Testing Station, Idaho Nuclear Corporation, Idaho Falls, Idaho 83401

(Received 17 May 1971)

The prompt γ-ray spectrum resulting from capture of 2-keV neutrons in natural lead samples was measured using the 2-keV neutron beam facility of the Materials Testing Reactor. Primary capture γ-ray lines resulting from neutron capture in both ^{204}Pb and ^{207}Pb were observed in this spectrum. From these data, and utilizing the 477-keV prompt γ rays resulting from the ^{10}B(n,α) reaction as a flux monitor, cross-section values of 1.8 ± 0.5 b and 3.2 ± 1.2 mb, respectively, were obtained for capture of these 2-keV neutrons in ^{204}Pb and ^{207}Pb. These data also provide additional information about the level scheme of ^{205}Pb, including the existence of a previously unreported level at 1748.4 keV, with spin of $\frac{1}{2}$ or $\frac{3}{2}$ and with probable negative parity. A value of 6731.7 ± 0.6 keV was obtained for the neutron binding energy of ^{205}Pb.

I. INTRODUCTION

Measurements of the 41-keV resonance in the neutron-capture cross section of ^{207}Pb utilizing both the ^{207}Pb(n,γ) reaction[1] and the inverse reaction[2,3] ^{208}Pb(γ,n), have indicated that this resonance has an asymmetric shape. Bowman, Baglan, and Berman (BBB)[2] were able to fit their data on the shape of this resonance peak using a model developed by Longo and Saporetti[4] in which both di-